

# Differential rotation models for late-type dwarfs and giants

L.L. Kitchatinov<sup>1,2</sup> and G. Rüdiger<sup>2</sup>

<sup>1</sup> Institute for Solar-Terrestrial Physics, P.O. Box 4026, Irkutsk, 664033, Russia (kit@iszf.irk.ru)

<sup>2</sup> Astrophysikalisches Institut Potsdam, An der Sternwarte 16, D-14482 Potsdam, Germany (lkitchatinov@aip.de; gruediger@aip.de)

Received 20 April 1998 / Accepted 9 December 1998

**Abstract.** A model for global circulation in outer stellar convection zones is applied to simulate the angular velocity dependence of differential rotation for two spectral classes, G2 and K5, of main-sequence dwarfs. Only the solar-type rotation laws with an increasing angular velocity from pole to equator and a relatively small rotation inhomogeneity in radius were found. Differential rotation for G2 is larger compared to K5, their angular velocities being equal. As the rotation period decreases from its solar value, the absolute value of the surface differential rotation decreases initially but changes to a slight increase for periods of several days. The meridional flow inside the convection zones is confined to thin boundary layers at the top and bottom with a typical velocity amplitude of about  $10 \text{ m s}^{-1}$ . Also a sequence of rotation laws for evolving  $2.5M_{\odot}$  star is produced. The predicted differential rotation is solar-like in structure and super-solar in amplitude. A comparison with observations is made and implications for dynamo theory of stellar activity are briefly discussed.

**Key words:** stars: activity – stars: late-type – stars: rotation

## 1. Motivation and scope

This paper extends our former simulations (Kitchatinov & Rüdiger 1995) of the stellar differential rotation to model its rotation rate and spectral type dependence.

Such work is highly motivated by recent observations of stellar rotation and magnetic activity (Baliunas et al. 1995; Donahue et al. 1996) including in particular such stars as AB Doradus rotating much faster than the Sun (Donati & Cameron 1997, Donati et al. 1999). As the differential rotation is a key parameter for stellar dynamos, it is most tempting to know it for this latter case of rapidly rotating stars showing high magnetic activity. Consequently, our simulations cover rotation periods from the solar value down to  $P_{\text{rot}}=1$  day.

Also a knowledge of the meridional flow would be important in constructing the stellar dynamos (Choudhury et al. 1995). The paper, therefore, concerns the model-predicted flow structure and its dependence on the rotation rate.

We present a series of differential rotation models for the main-sequence dwarfs of spectral types G2 (the Sun) and K5.

*Send offprint requests to:* L.L. Kitchatinov

As the period,  $P_{\text{rot}}$ , decreases, the absolute value of the surface differential rotation drops initially but changes to a very smooth increase for the shortest  $P_{\text{rot}}$ . In the scaling relation,

$$\frac{\Delta\Omega}{\Omega} = \frac{\Omega_{\text{eq}} - \Omega_{\text{pole}}}{\Omega_0} \sim \Omega^{-n'}, \quad (1)$$

the power index  $n'$  defines the decay of the relative differential rotation with the basic rotation.  $n' = 0.3$  according to Donahue et al. (1996), but with the rapidly rotating AB Dor involved it should reach the value of  $n' \simeq 1$ .

Another type of convective stars to which the differential rotation theory may apply are the giants of luminosity class III. Observations revealed several striking regularities concerning rotation and magnetic activity of the evolved stars. The rotational discontinuity known for mid-F main-sequence dwarfs is also observed for early-G giants (Gray 1989a). Later on, the rotation rate is uniquely defined by the spectral type. Similar to the Sun, magnetic activity is confined to the equatorial belts (Gray 1989b, 1991).

The observational findings may be interpreted in terms of convective dynamos and magnetic braking. No dynamo models for giants have been developed so far, however. As a first step in this direction we generate a sequence of differential rotation models covering the evolution of a  $2.5M_{\odot}$  star from about G2 to K1 which are roughly the spectral types where a drastic change in rotation rates and the disappearance of the indicators for hot coronas are observed. The hydromagnetic dynamo is supposed to work in this range between the rotational and coronal boundaries (Gray 1991).

## 2. The model

The model relies on the mean-field approach to the hydrodynamics of rotating turbulent fluids (Rüdiger 1989). It defines the global axisymmetric flow and heat transport in a spherical convective shell.

### 2.1. Basic equations

The equation for the steady mean velocity field,  $\mathbf{u}$ ,

$$(\mathbf{u} \cdot \nabla) \mathbf{u} + \frac{1}{\rho} \nabla p - \mathbf{g} = -\frac{1}{\rho} \text{div} (\rho \hat{Q}), \quad (2)$$

includes the effects of turbulence through the one-point correlation tensor,  $\hat{Q}$ , of the fluctuating velocities,  $\mathbf{u}'$ ,

$$Q_{ij} = \langle u'_i(\mathbf{r}, t) u'_j(\mathbf{r}, t) \rangle, \quad (3)$$

where  $p$  is mean pressure,  $\rho$  is density, and  $\mathbf{g}$  is gravity.

The tensor (3) splits into a non-diffusive part,  $\hat{Q}^\Lambda$ , representing the mean momentum fluxes by rotating turbulence (the  $\Lambda$ -effect), and the eddy viscosity term (Rüdiger 1989):

$$Q_{ij} = Q_{ij}^\Lambda - \mathcal{N}_{ijkl} \frac{\partial u_k}{\partial r_l}. \quad (4)$$

The present model adopts the results of our previous derivations of the convective angular momentum fluxes (Kitchatinov and Rüdiger 1993) and the eddy transport coefficients for rotating fluids (Kitchatinov et al. 1994). The main assumption of that derivations on the turbulence nature was that the original turbulence is quasi-isotropic, i.e., the sole source of its anisotropy is the fluid inhomogeneity. The influence of the basic rotation on the original turbulence was described within the SOCA-approximation of the mean-field theory to account for the turbulence distortion by the Coriolis forces. No limitations on the rotation rate were imposed to derive fully nonlinear dependencies on the angular velocity. In particular, the eddy viscosity tensor,

$$\begin{aligned} \mathcal{N}_{ijkl} = & \nu_1 (\delta_{ik} \delta_{jl} + \delta_{jk} \delta_{il}) \\ & + \nu_2 (\delta_{il} \hat{\Omega}_j \hat{\Omega}_k + \delta_{jl} \hat{\Omega}_i \hat{\Omega}_k \\ & + \delta_{ik} \hat{\Omega}_j \hat{\Omega}_l + \delta_{jk} \hat{\Omega}_i \hat{\Omega}_l + \delta_{kl} \hat{\Omega}_i \hat{\Omega}_j) \\ & + \nu_3 \delta_{ij} \delta_{kl} - \nu_4 \delta_{ij} \hat{\Omega}_k \hat{\Omega}_l + \nu_5 \hat{\Omega}_i \hat{\Omega}_j \hat{\Omega}_k \hat{\Omega}_l, \end{aligned} \quad (5)$$

allows for the rotationally-induced anisotropy and quenching. In Eq. (5),  $\hat{\Omega} = \mathbf{\Omega}/\Omega$  is the unit vector parallel to the rotation axis,  $\mathbf{\Omega}$  is the angular velocity, and the viscosity coefficients,  $\nu_n$ , depend on the rotation rate,

$$\nu_n = \nu_T \phi_n(\Omega^*), \quad (6)$$

through the functions  $\phi_n(\Omega^*)$  of the local Coriolis number,

$$\Omega^* = 2\tau\Omega, \quad (7)$$

where  $\tau$  is the convective turn-over time. The viscosity,  $\nu_T$ , for the nonrotating fluid is defined in terms of the intensity,  $\langle u_0'^2 \rangle$ , of the original turbulence:

$$\nu_T = \frac{4}{15} \tau \langle u_0'^2 \rangle. \quad (8)$$

We keep here the same notations for the quenching functions,  $\phi_n(\Omega^*)$ , as in Kitchatinov et al. (1994) where the explicit expressions for the functions may be found. For a nonrotating fluid,  $\Omega^* = 0$ , the functions  $\phi_2$ ,  $\phi_4$  and  $\phi_5$  fall to zero, and Eq. (5) reduces to the isotropic eddy viscosity.

The quantity  $\langle u_0'^2 \rangle$  in Eq. (8) stands for the intensity of the so-called original turbulence which would take place under actual sources of turbulence (actual superadiabaticity), but if

rotation were absent. In accord with the definition, the mixing-length relation for nonrotating fluids can be used to define the intensity,

$$\langle u_0'^2 \rangle = -\frac{\ell^2 g}{4c_p} \frac{\partial S}{\partial r}, \quad (9)$$

where  $S$  is specific entropy,  $\ell$  is the mixing length, and  $c_p$  is heat capacity at constant pressure. The entropy gradient in (9) is not prescribed but governed by the heat transport equation as discussed below.

On using the usual spherical coordinates,  $r$ ,  $\theta$  and  $\varphi$ , the steady axisymmetric mean velocity field may be written as

$$\mathbf{u} = \mathbf{i}_\varphi r \sin \theta \Omega + \frac{1}{\rho} \text{rot} \left( \frac{\mathbf{i}_\varphi \Psi}{r \sin \theta} \right), \quad (10)$$

where  $\Psi$  is the stream function for the meridional flow and  $\mathbf{i}_\varphi$  is the azimuthal unit vector. The zonal component of Eq. (2) gives the equation,

$$\begin{aligned} \frac{\sin \theta}{r^2} \frac{\partial}{\partial r} (\rho r^3 Q_{r\varphi}) + \frac{1}{\sin \theta} \frac{\partial}{\partial \theta} (\rho \sin^2 \theta Q_{\theta\varphi}) \\ + \frac{\sin \theta}{r^2} \frac{\partial \Psi}{\partial \theta} \frac{\partial (r^2 \Omega)}{\partial r} - \frac{1}{\sin \theta} \frac{\partial \Psi}{\partial r} \frac{\partial (\sin^2 \theta \Omega)}{\partial \theta} = 0, \end{aligned} \quad (11)$$

describing the angular momentum transport by turbulence and by the meridional flow. Our previous derivations of  $\hat{Q}^\Lambda$  (Kitchatinov & Rüdiger 1993) and Eqs. (5)-(9) yield the following expressions for the correlation tensor components of Eq. (11)

$$\begin{aligned} Q_{r\varphi} = & \sin \theta \frac{\tau \ell^2 g}{15c_p} \frac{\partial S}{\partial r} \left\{ \phi_1(\Omega^*) r \frac{\partial \Omega}{\partial r} \right. \\ & + \phi_2(\Omega^*) \cos \theta \left( \cos \theta r \frac{\partial \Omega}{\partial r} - \sin \theta \frac{\partial \Omega}{\partial \theta} \right) \\ & \left. - \Omega \left( \frac{\alpha_{\text{MLT}}}{\gamma} \right)^2 (\mathcal{I}_0(\Omega^*) + \cos^2 \theta \mathcal{I}_1(\Omega^*)) \right\}, \\ Q_{\theta\varphi} = & \sin \theta \frac{\tau \ell^2 g}{15c_p} \frac{\partial S}{\partial r} \left\{ \phi_1(\Omega^*) \frac{\partial \Omega}{\partial \theta} \right. \\ & + \phi_2(\Omega^*) \sin \theta \left( \sin \theta \frac{\partial \Omega}{\partial \theta} - \cos \theta r \frac{\partial \Omega}{\partial r} \right) \\ & \left. + \Omega \left( \frac{\alpha_{\text{MLT}}}{\gamma} \right)^2 \sin \theta \cos \theta \mathcal{I}_1(\Omega^*) \right\}, \end{aligned} \quad (12)$$

where  $\alpha_{\text{MLT}}$  is the proportionality constant between the mixing length and pressure scale height,  $\ell = \alpha_{\text{MLT}} H_p$ , and  $\gamma$  is the adiabaticity index. In Eqs. (12) we keep the same notations for the functions of  $\Omega^*$  as in the papers (Kitchatinov & Rüdiger 1993; Kitchatinov et al. 1994) where these functions are given.

The meridional forces balance is governed by the vorticity equation which results from the zonal component of the curled Eq. (2):

$$\mathcal{D}(\Psi) = \sin \theta r \frac{\partial \Omega^2}{\partial z} + \frac{1}{\rho^2} (\nabla \rho \times \nabla p)_\varphi, \quad (13)$$

where  $\partial/\partial z = \cos\theta\partial/\partial r - r^{-1}\sin\theta\partial/\partial\theta$  is the spatial derivative along the rotation axis. The left side of Eq. (13) represents the viscous damping of the meridional flow:

$$\mathcal{D}(\Psi) = -\varepsilon_{\varphi jk} \frac{\partial}{\partial r_j} \left( \frac{1}{\rho} \frac{\partial}{\partial r_l} \rho \mathcal{N}_{klmn} \frac{\partial u_m}{\partial r_n} \right). \quad (14)$$

The explicit expression for  $\mathcal{D}(\Psi)$  in spherical coordinates is too complicated to reproduce here. One can obtain the expression from Eqs. (5), (10), and the definition (14).

From the ideal gas entropy expression,  $S = c_v \ln(p/\rho^\gamma)$ , we find

$$\frac{\nabla \rho}{\rho} = -\frac{\nabla S}{c_p} + \frac{\nabla p}{\gamma p}. \quad (15)$$

The barocline term on the right of Eq. (13) can, then, be transformed as

$$\frac{1}{\rho^2} (\nabla \rho \times \nabla p)_\varphi = -\frac{1}{c_p \rho} (\nabla S \times \nabla p)_\varphi = -\frac{g}{c_p r} \frac{\partial S}{\partial \theta}, \quad (16)$$

where the final expression neglects a small rotational asphericity in the distribution of pressure. The meridional flow equation (13) now reads

$$\mathcal{D}(\Psi) = \sin\theta r \frac{\partial \Omega^2}{\partial z} - \frac{g}{c_p r} \frac{\partial S}{\partial \theta}. \quad (17)$$

Next, the heat transport equation,

$$\text{div}(\mathbf{F}^{\text{conv}} + \mathbf{F}^{\text{rad}}) + \rho T \mathbf{u} \cdot \nabla S = 0. \quad (18)$$

is involved to close the equation system. The equation neglects the source-term by viscous heating but allows for the heat transport by convection,

$$\mathbf{F}_i^{\text{conv}} = -\rho T \chi_{ij} \frac{\partial S}{\partial r_j}, \quad (19)$$

by radiation,

$$\mathbf{F}^{\text{rad}} = -c_p \rho \chi_D \nabla T, \quad \chi_D = \frac{16\sigma T^3}{3\kappa \rho^2 c_p}, \quad (20)$$

and by the meridional flow.

The eddy conductivity tensor includes the rotationally induced anisotropy and quenching:

$$\chi_{ij} = -\frac{\tau \ell^2 g}{12c_p} \frac{\partial S}{\partial r} \left( \phi(\Omega^*) \delta_{ij} + \phi_{\parallel}(\Omega^*) \hat{\Omega}_i \hat{\Omega}_j \right), \quad (21)$$

where once again we keep the same notations for the conductivity quenching functions,  $\phi$ ,  $\phi_{\parallel}$ , as in the paper where the functions have been derived (Kitchatinov et al. 1994).

We adopt the Kramers' opacity law,  $\kappa = c_\kappa \rho T^{-7/2}$ , in the radiative conductivity (20). The  $c_\kappa$ -value is adjusted to reproduce the position of the convection zone base supplied by a stellar structure model. E.g.,  $c_\kappa = 2.04 \cdot 10^{24}$  cgs for the Sun with the base at  $0.73R_\odot$ . The choice of  $c_\kappa$  is equivalent to an adjustment to the chemical composition of a star, the opacity being much sensitive to the content of heavy elements. The radiative heat transport was, however, neglected when computing the differential rotation of giants in view of highly non-uniform chemical composition of the evolved stars.

## 2.2. The model design and the stellar parameters

The model defines the differential rotation, meridional circulation and entropy distributions in a spherical convective shell by solving numerically the system of Eqs. (11), (17), and (18).

The computation domain does not extend up to the surface of the star but has an external boundary ( $r_e$ ) placed a few percent of the stellar radius below photosphere. This is partly dictated by numerical difficulties arising due to a very sharp near-surface stratification and partly by an internal contradiction of the mixing-length formalism: the mixing-length models supply the effective diffusivities for which the upper layers of a star are still unstable to thermal convection (Tuominen et al. 1994). The models for giants suffer from the instability exceptionally much. To exclude the instability, the heat transport by the meridional flow was neglected when simulating the global circulation in giants. Possible consequences of the neglect were estimated by recomputing several (stable) models of the main-sequence dwarfs with the heat transport by meridional flow also neglected. The results changed rather little.

The thermal boundary condition at  $r = r_e$  assumes the surface layer beyond  $r_e$  to be an efficient heat exchanger such that the total heat flux,  $F_r$ , on the boundary matches the black body radiation of the photosphere (Gilman & Glatzmaier 1981),

$$F_r = \frac{L}{4\pi r_e^2} \left( 1 + 4 \frac{\delta T}{T_{\text{eff}}} \right) \quad \text{at } r = r_e, \quad (22)$$

where  $L$  is the stellar luminosity,  $T_{\text{eff}}$  is the surface effective temperature, and  $\delta T = T \delta S / c_p$  is the temperature disturbance at the external boundary. The other boundary conditions assume the constant heat flux on the internal boundary ( $r_i$ ), zero stress and no penetration on both boundaries:

$$\begin{aligned} F_r &= \frac{L}{4\pi r_i^2}, \quad \text{at } r = r_i \\ \Psi &= 0, \quad Q_{r\varphi} = Q_{r\theta} = 0 \quad \text{at } r = r_i \quad \text{and } r = r_e. \end{aligned} \quad (23)$$

Stratification in the deep of stellar convection zones is known to be very close to adiabaticity. We neglect the deviations from adiabatic profiles in all the thermodynamic parameters except, of course, the entropy gradient (and  $\delta T$  in Eq. (22)). The values of thermodynamic parameters at some location inside the convection zone are required, however, to define the adiabatic profiles. To this end, the density ( $\rho_e$ ) and temperature ( $T_e$ ) at the external boundary were taken from an appropriate stellar structure model.

The convective turnover time profile,

$$\tau = \left( \frac{16\pi r^2 c_p T \rho \ell^2}{3gL} \right)^{1/3}, \quad (24)$$

is assumed independent of the rotation rate.

The model requires nine input parameters to be specified in order to define a particular star for the simulations. Apart from  $\rho_e$  and  $T_e$ , the parameters include the radius ( $R$ ), mass ( $M$ ), luminosity ( $L$ ), fractional radii of the convection zone bottom ( $x_i$ ) and external boundary ( $x_e$ ) of the simulation domain, the

**Table 1.** Input stellar parameters

Star	$M/M_\odot$	$L/L_\odot$	$R/R_\odot$	$\rho_e$ , g cm $^{-3}$	$T_e$ , K	$x_i$
G2	1	1	1	$7.46 \cdot 10^{-3}$	$2.86 \cdot 10^5$	0.73
K5	0.7	0.133	0.644	$6.77 \cdot 10^{-2}$	$3.43 \cdot 10^5$	0.69

**Table 2.** Input parameters for evolving star of  $2.5M_\odot$ 

N $_o$	$T_{\text{eff}}$ , K	$R/R_\odot$	$\rho_e$ , g cm $^{-3}$	$T_e$ , K	$x_i$	$\Omega_o$ , s $^{-1}$
1	5413	7.96	$2.56 \cdot 10^{-5}$	$7.94 \cdot 10^4$	0.69	$1.17 \cdot 10^{-6}$
2	5236	7.91	$5.69 \cdot 10^{-5}$	$8.07 \cdot 10^4$	0.61	$1.07 \cdot 10^{-6}$
3	5016	8.88	$6.75 \cdot 10^{-5}$	$7.23 \cdot 10^4$	0.47	$7.48 \cdot 10^{-7}$
4	4900	10.3	$4.40 \cdot 10^{-5}$	$6.00 \cdot 10^4$	0.36	$4.98 \cdot 10^{-7}$
5	4794	12.1	$2.83 \cdot 10^{-5}$	$5.14 \cdot 10^4$	0.27	$3.63 \cdot 10^{-7}$
6	4689	14.6	$1.38 \cdot 10^{-5}$	$3.93 \cdot 10^4$	0.177	$2.73 \cdot 10^{-7}$

mixing-length parameter ( $\alpha_{\text{MLT}} = \ell/H_p$ ), and the latitude-averaged angular velocity,

$$\bar{\Omega} = \frac{3}{4} \int_0^\pi \Omega \sin^3 \theta \, d\theta, \quad (25)$$

of the surface ( $\Omega_o$ ). Eq. (25) gives the angular momentum–corresponding average, i.e. the angular momentum redistribution in latitude does not change the  $\bar{\Omega}$ .

From the input parameters, only  $\alpha_{\text{MLT}}$  is to some extent free. Computations for the Sun (Kitchatinov & Rüdiger 1995) have shown, however, that the model predictions react on the variations of  $\alpha_{\text{MLT}}$  only slightly.  $x_e = 0.95$  and  $\alpha_{\text{MLT}} = 1.7$  throughout this paper. The other input parameters for the considered main–sequence stars are given in Table 1.

The red giant in our simulations is the star of  $2.5M_\odot$ . The input parameters of Table 2 were taken from the evolutionary model by Herwig et al. (1997). The table shows also the mean angular velocity estimated from the empirical law Gray (1989a),

$$u_{\text{eq}} = 7.31 - 0.417\text{Sp}, \quad (26)$$

where  $u_{\text{eq}}$  is the equatorial rotation rate in km s $^{-1}$ , Sp is the numerical spectral type equal to 3 for G3, 4 for G4, ..., 10 for K0, .... Six parameter sets of Table 2 cover the stellar evolution from about G2 to K1, i.e. approximately the range between rotational and coronal boundaries (cf. Gray 1991).

### 2.3. Preliminary estimations

An important observation with Eq. (17) is that the relative value of the first term on the right to the term on the left is the Taylor number

$$\text{Ta} = \frac{4\Omega^2 R^4}{\nu_T^2} \approx 10\Omega^{*2} (R/\ell)^4. \quad (27)$$

(cf., e.g., Brandenburg et al. 1990). Already for the Sun, the Taylor number is large,  $\text{Ta} \simeq 10^7$ . It increases further for faster rotating G2 and for K5 ( $\tau$  increases for later spectral types, Durney & Latour 1978). The viscous drag to the meridional flow can

be neglected in Eq. (17) for the rapidly rotating stars with large Taylor numbers with the consequence that the nonpotential part of the centrifugal force should be almost balanced by the barocline force in the bulk of convection zone (Durney 1987, 1989). If we further assume that the angular velocity inhomogeneity along the rotation axis can be estimated as

$$\frac{\partial\Omega}{\partial z} \approx \frac{\Delta\Omega}{R}, \quad (28)$$

then Eq. (17) leads to the estimation,

$$\frac{\Delta\Omega}{\Omega} \approx \frac{g\nabla S}{\Omega^2 c_p} \approx \frac{u'^2}{\ell^2 \Omega^2 \sqrt{\phi(\Omega^*)}}, \quad (29)$$

where  $\phi(\Omega^*)$  is the eddy conductivity quenching function (cf. Eq. (21)).  $\phi(\Omega^*) \sim 1/\Omega^*$  for  $\Omega^* \gg 1$  (Kitchatinov et al. 1994). Assuming further that  $\tau \sim \ell/u'$  we finally get

$$\frac{\Delta\Omega}{\Omega} \approx \frac{4}{\Omega^{*3/2}}. \quad (30)$$

Though rather rough, the estimation (30) agrees with subsequent numerical simulations for not too high  $\Omega^*$  (the barocline term in Eq. (17) becomes insignificant for very large  $\Omega^*$ , and the estimation (28) is violated). The estimation leads to two important consequences. Firstly, the relative value of the differential rotation is a decreasing function of rotation rate for a given spectral type (given  $\tau$ ). With increasing stellar age, the rotation becomes more and more nonuniform.

Secondly, for a given angular velocity, the stars of later spectral types are expected to rotate more rigidly because of an increase in convective turnover time with decreasing stellar mass and the resulting increase of the Coriolis number. E.g., the  $\tau$ -values for K5 are about two times larger compared with G2.

The estimations show that the case of a relatively fast and strongly non-uniform rotation cannot be found between the main-sequence dwarfs. The case may, however, well be expected for the red giants. All the models of Table 2 have almost the same  $\Omega^* \sim 4$  (in the middle of convection zone) slightly below  $\Omega^* \simeq 6$  for the Sun and the (linear) rotation rates above the solar value. The expectation was one of the reasons to model the differential rotation for giants.

Dwarfs with the shortest rotation periods present difficulties for numerical simulations. The balance of the centrifugal and barocline forces (discussed above) contradicts the stress-free boundary conditions (23). The boundary layers with thickness  $h \approx R\text{Ta}^{-1/4}$  develop on the top and bottom of the spherical shell (Durney 1989). The angular velocity changes only slightly inside the layers but the angular velocity gradient varies sharply and the meridional flow is highly concentrated to the top and bottom. We did not find a possibility to sidestep the layers problem, e.g., by accounting their effect through a modification in the boundary conditions or somehow else. Very high numerical resolution over radius was required in view of a pure a priori knowledge of the layers structure. In the most extreme case of K5 with  $P_{\text{rot}} = 1$  day, as many as  $10^4$  radial grid points were required to get the resolution-independent result. An example for the layers is given in the next section.

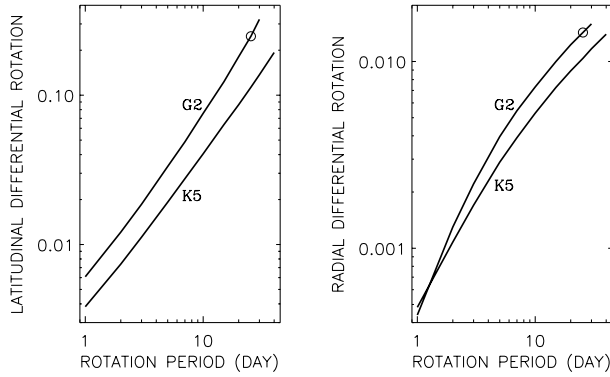


**Fig. 1.** The rotation inhomogeneities over latitude (*left*) and radius (*right*) for the MS dwarfs G2 and K5, cf. Eqs. (1) and (31). The circles represent the Sun

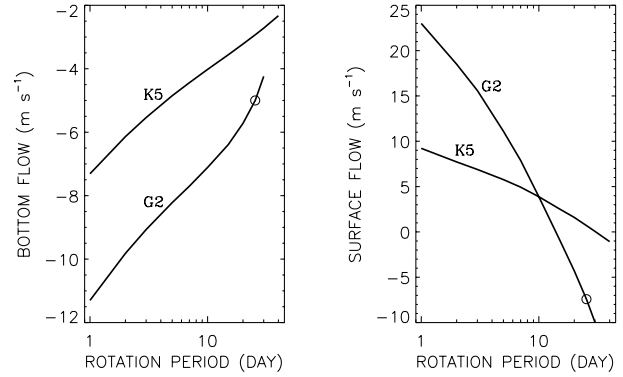


**Fig. 2.** Meridional flow at 45°-latitude at the bottom (*left*) and top (*right*) as a function of rotation period. The positive values correspond to a poleward flow. The circles represent the solar case

### 3. Results and discussion

#### 3.1. Dwarfs

Fig. 1 shows the simulated equator-to-pole angular velocity variations (1) on the stellar surface,  $\Delta\Omega/\Omega$ , and the latitude-averaged rotation inhomogeneity with depth,

$$\left. \frac{\Delta\Omega}{\Omega} \right|_{\text{rad}} = \frac{\bar{\Omega}_{\text{bot}} - \Omega_0}{\Omega_0}, \quad (31)$$

as functions of the rotation period. Remember that  $\Omega_0$  is the latitude-averaged angular velocity at the surface and the averaging is defined by Eq. (25). As expected, the differential rotation grows with  $P_{\text{rot}}$  and it is smaller for K5-star compared to G2. For all computed models, the rotation rate increases from poles to equator and from top to bottom. The radial inhomogeneities are very small.

With rotation period increasing beyond the range shown in Fig. 1, the latitudinal differential rotation of G2 initially saturates at the value of about 50% and even starts decreasing with  $P_{\text{rot}}$  for  $P_{\text{rot}} \gtrsim 150$  days. Such long rotation periods are of no practical interest, however.

Application of the power law  $\Delta\Omega/\Omega \sim \Omega^{-n'}$  (1) usually used to fit observational data, to the results of Fig. 1 shows that the power index,  $n'$ , is not constant but decreases from  $n' = 1.56$  for the solar rotation period to  $n' = 1$  for  $P_{\text{rot}} = 1$  day. The mean value for the entire period range is  $n' = 1.15$ , all for G2. The  $n'$ -values for K5 equal 1.21, 0.95, and 1.04 respectively. The slope  $n' \simeq 1$  for rapid rotators is not far from  $n' = 0.85$  found by Hall (1991). Our  $n'$ -values are, however, considerably larger than  $n' = 0.3$  reported by Donahue et al. (1996) and Rüdiger et al. (1998). The disagreement may be partly due to the sample by Donahue et al. (1996) combined different spectral types. The longest rotation periods were represented mainly by K-stars and the shortest ones – by G-stars. Therefore, the dependence of the differential rotation on  $P_{\text{rot}}$  derived from that sample may change from the upper line in the left of Fig. 1 at small periods to the lower line for large  $P_{\text{rot}}$  to reduce the slope  $n'$ .

Donati & Cameron (1997) found  $\Delta\Omega/\Omega \simeq 4.6 \cdot 10^{-3}$  for very rapidly rotating K0 dwarf AB Dor (cf. also Donati et al.

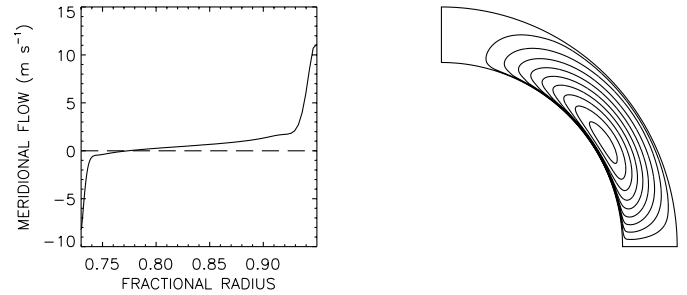


**Fig. 3.** An example of the boundary layers for the G2 star with  $P_{\text{rot}} = 5$  days. The left panel shows the depth profile of the horizontal velocity at 45°-latitude. The positive velocity means a poleward flow. The right panel shows the stream lines

1999). By extrapolating the plots of Fig. 1 to the rotation period  $P_{\text{rot}} \simeq 0.5$  day of AB Dor we find about two times smaller differential rotation. Not a poor agreement, perhaps, for the extreme case.

Apart from the differential rotation, the global meridional flow may be important for stellar dynamos (Choudhury et al. 1995). Fig. 2 shows the flow amplitudes at the top and bottom of convective envelope. The bottom velocity for the Sun,  $u_m \simeq 5 \text{ m s}^{-1}$ , suffices to influence the latitudinal migration of the magnetic field over the solar cycle. The equatorward surface flow does not agree with solar observations (Howard 1984). Note, however, that the surface flow changes to poleward direction for rotation periods shorter than about 15 days.

A typical example of the meridional flow pattern is shown in Fig. 3 which illustrates also the boundary layers discussed in the preceding section. The flow concentrates in the top and bottom layers with roughly the same velocity amplitudes.

The decrease in differential rotation with angular velocity may result in a change of the stellar dynamo from the  $\alpha\Omega$  regime to the  $\alpha^2\Omega$  or even  $\alpha^2$  mechanism with increasing rotation rate. The  $\alpha^2$ -dynamos normally produce steady but nonaxisymmetric magnetic fields (Rüdiger & Elstner 1994). This may explain why the rapidly rotating young stars do not exhibit the activity cycles (Baliunas et al. 1995).

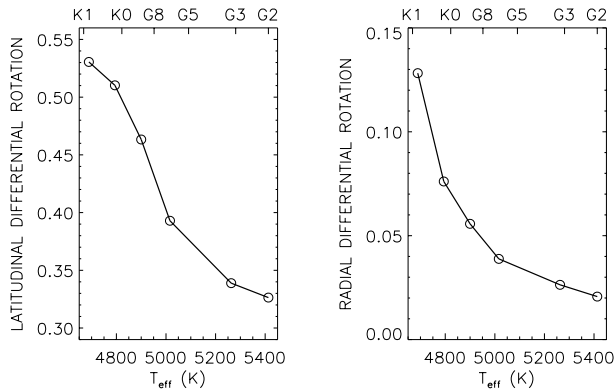


**Fig. 4.** The rotation inhomogeneity over latitude (*left*) and radius (*right*) as functions of effective surface temperature of the evolving giant. Cf. Eqs. (1) and (31). The estimated spectral types are indicated on the top. The circles show the actually computed points

### 3.2. Giants

In contrast to the main-sequence dwarfs, the model-predicted differential rotation of giants is large. Fig. 4 shows the results for the sequence of evolutionary stages of Table 2. Already for G2 the rotation inhomogeneity exceeds the solar value. It increases further as the star evolves to later spectral types. Note that the rotation rates of the red giants are defined by the observation-based relation (26).

As discussed above, the strongly non-uniform rotation may be related to the moderate Coriolis numbers. Estimations for the middle of convection zone give the number varying rather slightly as  $\Omega^* \simeq 3.2, 3.9, 5.3, 4.4, 3.6, 2.9$  from G2 to K1. The near-constancy of  $\Omega^*$  may be an explanation for the moderate variation of the latitudinal differential rotation in Fig. 4 in spite of the about fivefold change in the rotation rate. The larger spread in the radial rotation inhomogeneities may be related to a change in the depth of convection zone.

Fig. 5 shows the global flow patterns for the evolutionary sequence of Table 2. Note that the stellar radius is scaled to unity on all panels so that we cannot see an almost twofold increase in the size of the star from row 1 to 6.

The differential rotation is solar-like for all of the models: the angular velocity increases strongly from pole to equator but varies only slightly with depth. In a further similarity, the diffusive times,  $t_d = R^2/\nu_T$ , for the giants are almost the same as that for the Sun (about one order of magnitude increase in radius is compensated for by an increase in the eddy viscosity). The similarity in rotation laws implies a similar dynamo regime. The giants are, indeed, observed to possess equatorial activity belts similar to those of the Sun (Gray 1989b, 1991). Long-term variations of magnetic activity resembling the solar cycle were also observed (Donahue 1996). The luminosity class III giants may be much more solar-like than the rapidly rotating main-sequence dwarfs.

It is not clear at this stage, however, to what extent the predicted differential rotation of giants may agree with observations.

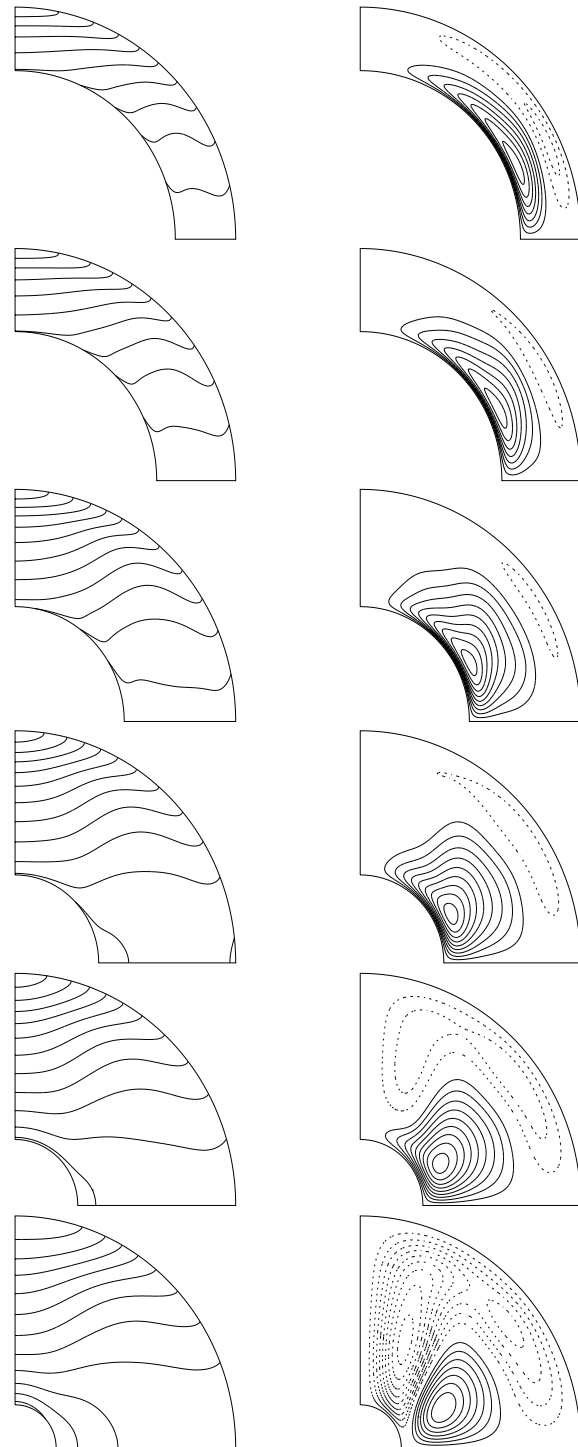


**Fig. 5.** Angular velocity isolines (*left*) and the meridional flow streamlines (*right*) for the sequence of giant models. The solid and dashed lines show the anticlockwise and clockwise circulation respectively. From top to bottom: models 1 to 6 of Table 2

*Acknowledgements.* The authors are grateful to Falk Herwig, Thomas Granzer, and Michael Stix for the possibility to use their models of stellar structure. This work was supported by the Deutsche Forschungsgemeinschaft and by the Russian Foundation for Basic Research (Project 96-02-00010)

**References**

- Baliunas S., Donahue R.A., Soon W.H., et al., 1995, *ApJ* 438, 269
- Brandenburg A., Moss D., Rüdiger G., Tuominen I., 1990, *Solar Phys.* 128, 243
- Choudhuri A.R., Schüssler M., Dikpati M., 1995, *A&A* 303, L29
- Donahue R.A., 1996, Long-term stellar activity. In: Strassmeier K.G., Linsky J.L. (eds.) *IAU Symp.* 176, *Stellar Surface Structure*. Kluwer, Dordrecht, p. 261
- Donahue R.A., Saar S.H., Baliunas S., 1996, *ApJ* 466, 384
- Donati J.-F., Cameron A.C., 1997, *MNRAS* 291, 1
- Donati J.-F., Cameron A.C., Hussain G.A.J., Semel M., 1999, *MNRAS* 302, 437
- Durney B.R., 1987, Generalization of mixing length theory to rotating convection zones and application to the Sun. In: Durney B.R., Sofia S. (eds.), *The Internal Solar Angular Velocity*. D. Reidel, Dordrecht, p. 239
- Durney B.R., 1989, *ApJ* 338, 509
- Durney B.R., Latour J., 1978, *GAFD* 9, 241
- Gilman P.A., Glatzmaier G.A., 1981, *ApJS* 45, 335
- Gray D.F., 1989a, *ApJ* 347, 1021
- Gray D.F., 1989b, *PASP* 101, 1126
- Gray D.F., 1991, Dynamo action in evolved stars. In: Tuominen I., Moss D., Rüdiger G. (eds.) *IAU Coll.* 130, *The Sun and Cool Stars: Activity, Magnetism, Dynamos*. Springer, Berlin, p. 336
- Hall D.S., 1991, Learning about the stellar dynamos from long-term photometry of starspots. In: Tuominen I., Moss D., Rüdiger G. (eds.) *IAU Coll.* 130, *The Sun and Cool Stars: Activity, Magnetism, Dynamos*. Springer, Berlin, p. 353
- Herwig F., Blöcker T., Schönberner D., El Eid M., 1997, *A&A* 324, L81
- Howard R., 1984, *ARA&A* 22, 131
- Kitchatinov L.L., Rüdiger G., 1993, *A&A* 276, 96
- Kitchatinov L.L., Rüdiger G., 1995, *A&A* 299, 446
- Kitchatinov L.L., Pipin V.V., Rüdiger G., 1994, *Astron. Nachr.* 315, 157
- Rüdiger G., 1989, *Differential rotation and stellar convection: Sun and solar-type stars*. Gordon & Breach, New York
- Rüdiger G., Elstner D., 1994, *A&A* 281, 46
- Rüdiger G., v. Rekowski B., Donahue R.A., Baliunas S.L., 1998, *ApJ* 494, 691
- Tuominen I., Brandenburg A., Moss D., Rieutord M., 1994, *A&A* 284, 259